Strongly Nucleophilic Rh^I Centre in Square-Planar Complexes with Terdentate (κ^3) 2,2′:6′,2′′-Terpyridine Ligands: Crystallographic, Electrochemical and Density Functional Theoretical Studies

Boke C. de Pater,[a] Hans-Werner Frühauf,[a] Kees Vrieze,[a] René de Gelder,[b] Evert J. Baerends,[c] Drew McCormack,[c] Martin Lutz,[d] Anthony L. Spek,[d] and František Hartl*[a]

Keywords: Rhodium / Tridentate ligands / X-ray diffraction / Cyclic voltammetry / Density functional calculations

Rh^I-terpyridine complexes have been unambiguously formed for the first time. The 2,2′:6′,2′′-terpyridine (tpy), 4′-chloro-2,2′:6′,2′′-terpyridine (4′-Cl-tpy) and 4′-(*tert*-butyldimethylsilyl-*ortho*-carboranyl)-2,2′:6′,2′′-terpyridine (carboranyl-tpy) ligands were used for successful syntheses and characterisation of the corresponding Rh^I complexes with halide co-ligands, [Rh(X)(4′-Y-terpyridine)] (X = Cl, Y = H, Cl, carboranyl; X = Br, Y = H). All four neutral Rh-tpy complexes are square planar, with Rh–X bonds in the plane of the 4′-Y-terpyridine ligands. Full characterisation of these dark blue, highly air-sensitive compounds was hampered by their poor solubility in various organic solvents. This is mainly due to the formation of π-stacked aggregates, as evidenced by the crystal structure of [Rh(Cl)(tpy)]; in addition, [Rh(Cl)(carboranyl-tpy)] merely forms discrete dimers. The (bonding) properties of the novel Rh^I-terpyridine complexes have been studied with single-crystal X-ray diffraction, (time-dependent) density functional theoretical (DFT) calculations, far-infrared spectroscopy, electronic absorption spectroscopy and cyclic voltammetry. From DFT calculations, the HOMO of the studied Rh^I-terpyridine complexes involves predominantly the metal centre, while the LUMO resides on the terpyridine ligand. Absorption bands of the studied complexes in the visible region (400–900 nm) can be assigned to MLCT and MLCT/XLCT transitions. The relatively low oxidation potentials of [Rh(X)(tpy)] (X = Cl, Br) point to a high electron density on the metal centre. This makes the Rh^I-terpyridine complexes strongly nucleophilic and (potentially) highly reactive towards various (small) substrate molecules containing carbon–halide bonds.

Introduction

Transition metal complexes containing terdentate nitrogen ligands (N−N−N) are of great interest both in the field of supramolecular chemistry[1,2] and catalysis. For example,[3] $[Pd(Me)(N-N-N)]^+$ complexes react rapidly with CO and subsequently with norbornadiene to produce $[Pd\{C_7H_8C(O)Me\}(N-N-N)]^+$ on the road to metal-bound polyketone fragments. Notably, the highest insertion rates are for complexes containing highly rigid ligands, e.g. dipyrido[4,3-*b*;5,6-*b*]acridine.[4] According to theoretical calculations,[5] this is most probably due to the rigidity of the ligand causing an increased strain in the metal complex itself, thereby facilitating intermediate bidentate coordination of the N−N−N ligand. These interesting findings initiated investigation of isoelectronic Rh^I compounds. Haarman et al. reported novel compounds [Rh(Cl)(2,6-[$C(R^1)=N-R^2)_2C_5H_3N$], containing fairly flexible 2,6-diiminopyridine ligands.[6–8] These complexes react readily with alkyl halides and oxygen owing to a strongly nucleophilic Rh^I centre.[6] The present article extends these studies to complexes with stronger σ-donating[9] and more rigid terpyridine ligands.

Since the first report on 2,2′:6′,2′′-terpyridine (tpy) by Morgan and Burstall,[10,11] the coordination chemistry of this ligand and its derivatives has been widely studied. They exhibit variable coordination modes to transition metals, viz. terdentate,[1] bidentate,[1,2] or monodentate.[12] Although complexes with many late transition metals are known,[1] only a few Rh-terpyridine complexes have been prepared, all of which contain rhodium(II) or rhodium(III)

[a] Institute of Molecular Chemistry, University of Amsterdam, Nieuwe Achtergracht 166, 1018 WV Amsterdam, The Netherlands,
Fax: (internat.) +31-20-5256456
[b] Department of Inorganic Chemistry, Faculty of Science, University of Nijmegen,
Toernooiveld 1, 6525 ED Nijmegen, The Netherlands
[c] Department of Theoretical Chemistry, Free University Amsterdam,
De Boelelaan 1083, 1081 HV Amsterdam, The Netherlands
[d] Bijvoet Centre for Biomolecular Research, Department of Crystal and Structural Chemistry, University of Utrecht,
Padualaan 8, 3584 CH Utrecht, The Netherlands

centres.[12−18] Electrochemical studies revealed stable rhodium(IV)- and oxorhodium(V)-terpyridine species.[16] Some rhodium(I) intermediates with terpyridine ligands have been proposed to participate in catalytic cycles,[19] but their formation has never been unambiguously established.

We report here, for the first time, syntheses, structures, spectroscopic, redox and bonding properties of four mononuclear square-planar Rh^I-terpyridine complexes. Due to the planar tpy skeleton, these compounds exhibit a strong tendency to π-stacking, which implies their low solubility. This is the main factor complicating their characterisation. Consequently, the bulky *tert*-butyldimethylsilyl-*o*-carboranyl group was placed at the C(4′)-position of the tpy ligand of the Rh^I-terpyridine species in the hope that such a sterically demanding substituent would lead to an increase in solubility.

Results

Syntheses of Complexes [Rh(X)(4′-Y-tpy)] (X = Cl, Y = H (1), Cl (3), *tert*-butyldimethylsilyl-*o*-carboranyl (4); X = Br, Y = H (2)]

The novel complexes **1**−**4** (Scheme 1) have been prepared by a ligand displacement reaction (Scheme 2). Characterisation by NMR techniques was problematic due to the poor solubility of the complexes. After scanning for 20 h (using C_6D_6 as solvent), only complex **4** gave an acceptable ^1H NMR spectrum (Figure 1). The C(6,6′′)-H signals of **4** were hidden under the benzene signal. The B−H signals, presumably spread over the range of 2−4 ppm, were not observable. The ^1H spectrum also contained additional signals of a minor species, probably a degradation product, since complex **4** is far less stable in organic solvents than **1**−**3**. The solubility of **1**−**4** in CD_3CN is lower than that in benzene and no acceptable ^1H NMR spectrum could be recorded. Finally, although the solubility of **1**−**4** in [D_6]EtOH and [D_6]DMF is similar to that in benzene, the ^1H NMR spectra only exhibited very broad signals.

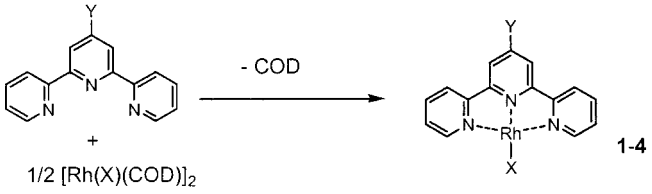

X = Cl (**1**,**3**,**4**), Br (**2**)
Y = H (**1**,**2**), Cl (**3**), *tert*-butyldimethylsilyl-*ortho*-carborane (**4**)
COD = cycloocta-1,5-diene

Scheme 2. Formation of complexes **1**−**4**

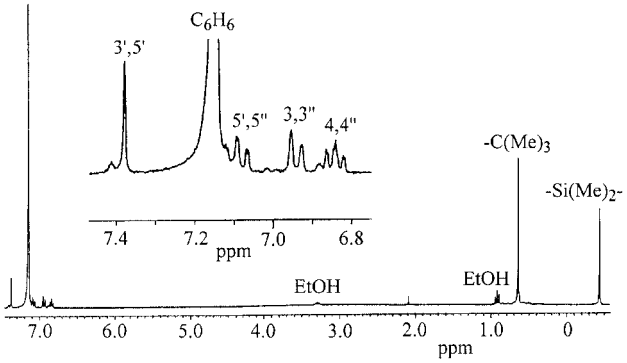

Figure 1. ^1H NMR spectrum of complex **4** in C_6D_6

X-ray Structures of Complexes 1 and 4

Molecules of complex **1** (Figure 2) are arranged in sheets that run parallel with the crystallographic *b*-axis (Figure 3). The sheets are 3.508(12) Å apart, which is considered as the thickness of the molecules. Neighbouring molecules in different sheets are in a staggered arrangement close to inversion symmetry. The distance between the sheets strongly indicates the presence of π-stacking (Figure 4). Within the sheets, short intermolecular distances are found between the chlorine atom and H5′ and H3′′ of a neighbouring molecule: H···Cl are 2.79 and 2.85 Å, and C−H···Cl angles 167° and 169°, respectively (Figure 5). These short distances

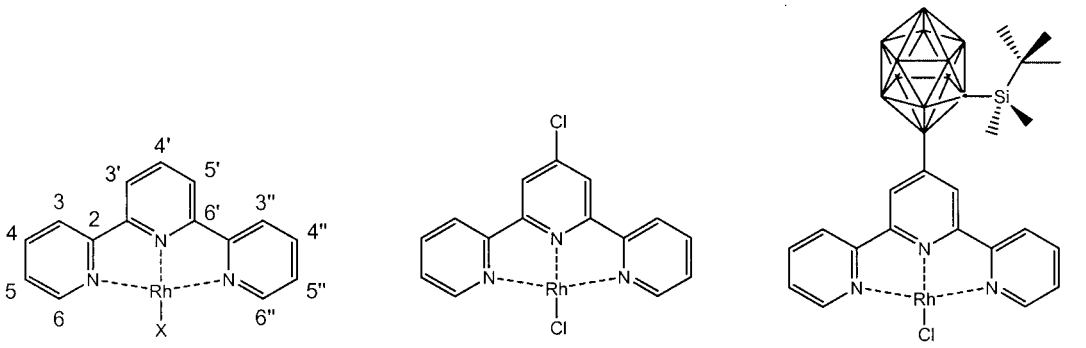

Scheme 1

indicate "chelating" C−H···Cl hydrogen bonds that link the neighbouring molecules into a one-dimensional intermolecular hydrogen-bonding network. The hydrogen-bonded sheets are stacked in the crystallographic [101] direction (Figure 5). There are no short Rh−Rh′ contacts, the smallest distance being 4.896(2) Å. Selected bond lengths and angles in complex **1**, together with those in the ADF/BP-calculated complexes **1′** and **2′**, for comparison, are summarised in Table 1 and Table 2, respectively.

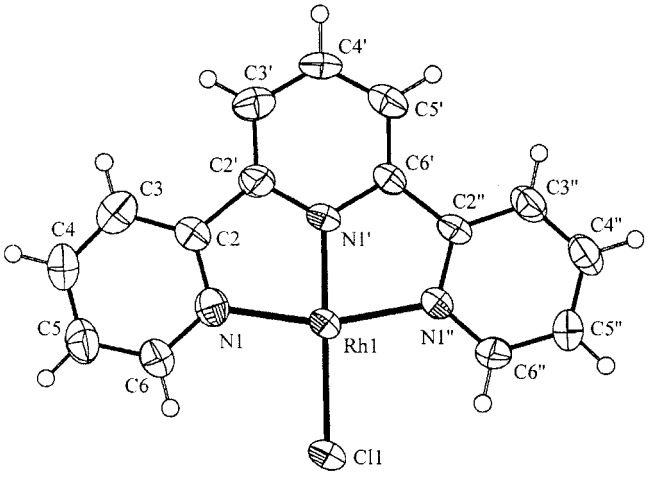

Figure 2. Displacement ellipsoid plot (50% probability level) of complex **1**

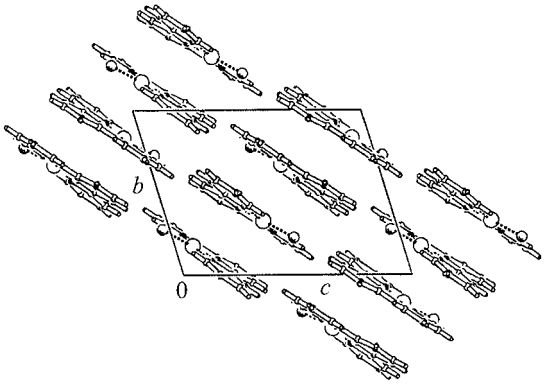

Figure 3. Molecular stacking in the crystal structure of complex **1**

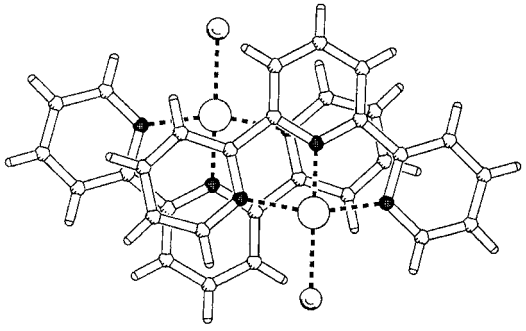

Figure 4. π-Stacking between two molecules in the crystal structure of complex **1**

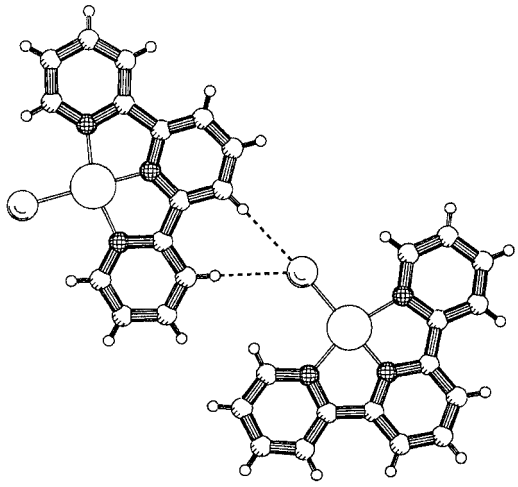

Figure 5. Hydrogen bonding in complex **1**

Table 1. Selected bond lengths (Å) for complexes **1** and **4**, and for geometry-optimised **1′** and **2′**

Bond length	**1**	**4**	**1′**	**2′**
Rh−X[a]	2.356(2)	2.369(2)	2.354	2.487
Rh−N1	2.026(7)	2.018(6)	2.048	2.057
Rh−N2	1.896(7)	1.890(6)	1.929	1.944
Rh−N3	2.019(7)	2.012(7)	2.048	2.057
N1−C1	1.336(12)	1.338(11)	1.350	1.350
N1−C5	1.362(12)	1.381(10)	1.381	1.381
N2−C6	1.360(11)	1.360(11)	1.371	1.370
N2−C10	1.354(11)	1.345(10)	1.371	1.370
N3−C11	1.367(11)	1.371(11)	1.381	1.381
N3−C15	1.347(11)	1.350(11)	1.350	1.350

[a] X = Cl for **1**, **4** and **1′**; Br for **2′**.

Table 2. Selected bond angles (°) for complexes **1** and **4**, and for geometry-optimised **1′** and **2′**.

Bond angles	**1**	**4**	**1′**	**2′**
X−Rh−N1[a]	99.5(2)	99.62(19)	99.8	100.2
X−Rh−N2	179.1(2)	175.1(2)	180.0	180.0
X−Rh−N3	99.1(2)	99.25(19)	99.8	100.2
N1−Rh−N2	80.8(3)	80.9(3)	80.2	79.8
N1−Rh−N3	161.3(3)	160.7(3)	160.3	159.6
N2−Rh−N3	80.5(3)	80.0(3)	80.2	79.8
Rh−N1−C1	128.9(7)	129.0(5)	127.7	127.8
Rh−N1−C5	113.2(6)	113.2(5)	113.5	113.6
C1−N1−C5	117.9(8)	117.8(6)	118.8	118.6
Rh−N2−C6	119.6(6)	118.8(5)	119.2	119.2
Rh−N2−C10	119.7(6)	120.1(5)	119.2	119.2
C6−N2−C10	120.7(8)	121.0(7)	121.6	121.6
Rh−N3−C11	113.5(5)	114.0(5)	113.5	113.6
Rh−N3−C15	128.6(6)	128.0(6)	127.7	127.8
C11−N3−C15	117.9(7)	117.9(7)	118.8	118.6

[a] X = Cl for **1**, **4** and **1′**; Br for **2′**.

Dark blue crystals of **4**, suitable for X-ray analysis, were grown from a saturated EtOH solution upon standing for three weeks at room temperature. In the solid state, the molecules (Figure 6) are packed in discrete dimers around the

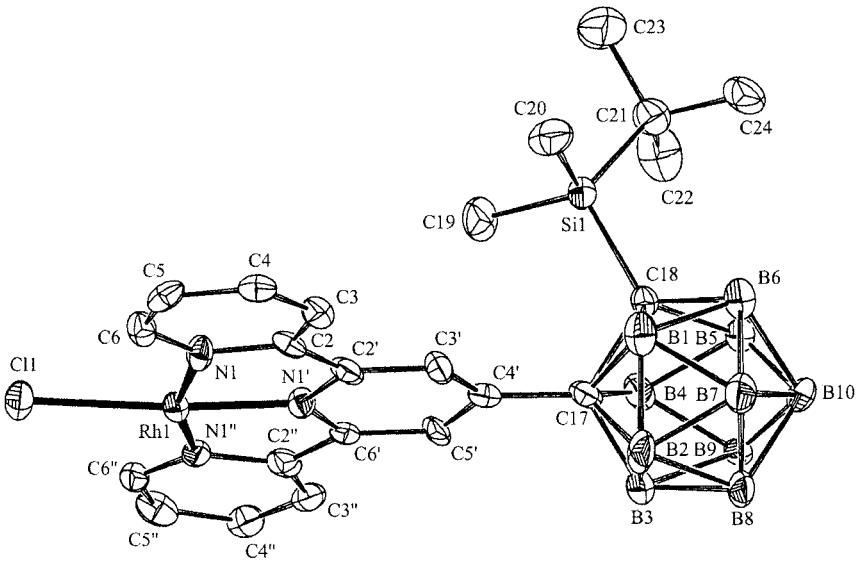

Figure 6. Displacement ellipsoid plot (50% probability level) of complex **4**. Hydrogen atoms and the disordered ethanol solvent molecule omitted for clarity

inversion centres (Figure 7), with Rh−Rh′ distances of 3.1503(13) Å. The packing of the dimers appears to be dominated by intermolecular hydrophobic interactions of the carborane residues, and by hydrophilic interactions of the Rh−Cl residues, with the disordered ethanol molecules also present in the structure. Apart from the interaction between the two halves of each dimer, no π-stacking is observed (Figure 8).

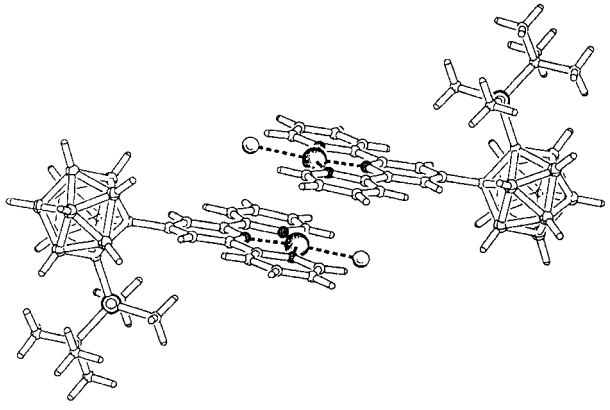

Figure 7. Dimer formation in the crystal structure of complex **4**. Symmetry operation i: $-x$, $1-y$, $1-z$

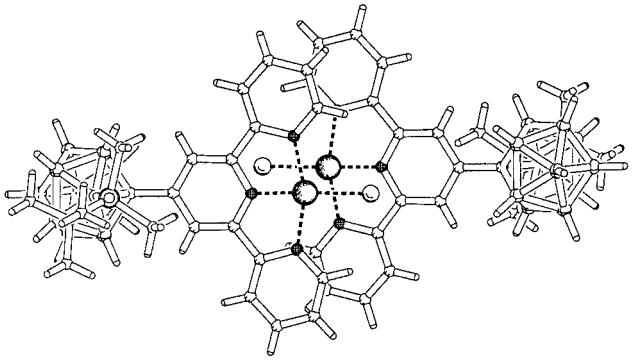

Figure 8. Perpendicular view of the aromatic system of complex **4**

FIR Spectra of Complexes 1 and 2

Generally, the IR ν(Rh−X) (X = Cl, Br) modes of pseudooctahedral $Rh^{III}X_3$-terpyridine complexes are difficult to assign.[20] The complexity of the FIR spectra of these complexes is largely attributed to the coupling of ν(Rh−X) and ν(Rh−N) modes, and to the difference between the ν(Rh−X) modes of the cis and trans halides.

Conversely, analysis of the square-planar Rh^{I}(X)-terpyridine complexes is easier. The FIR spectra of complexes **1** and **2** are similar, except for the ν(Rh−Cl) and ν(Rh−Br) bands (Figure 9). Assignment of ν(Rh−X) (X = Cl, Br for **1** and **2**, respectively) is straightforward: ν(Rh−Cl) at 256−260 cm^{-1} and ν(Rh−Br) at 188 cm^{-1}. The assignment of ν(Rh−Cl) is also supported by the observation of chlorine isotope splitting; the experimental value of 4 cm^{-1} (256 and 260 cm^{-1} for ^{37}Cl and ^{35}Cl, respectively) is similar to the calculated isotope splitting of 5 cm^{-1} ($K = 6.33\cdot10^{28}$ dyn cm^{-1} for $^{103}Rh-^{37}Cl$; 1 dyn = 10^{-3} N m^{-1} = 10^{-3} J).

The band pattern observed for complex **1** at 129 and 138 cm^{-1} is also considerably shifted to smaller wavenumbers for complex **2** (85 and 96 cm^{-1}). These bands are probably Rh−X bending vibrations (out-of-plane and in-plane).

Other absorption bands for **1** at 300−320, 220−230 and 153 cm^{-1} show only a minor shift to smaller wavenumbers for **2**, viz. 295−302, 214−226 and 141 cm^{-1}, respectively. These bands are attributed, without detailed analysis, to Rh−N/tpy vibrations.

DFT Study and Electronic Absorption Spectra of Complexes 1 and 2

Density functional theoretical calculations were performed on complexes **1** and **2**, restricted to a C_{2v}-symmetry

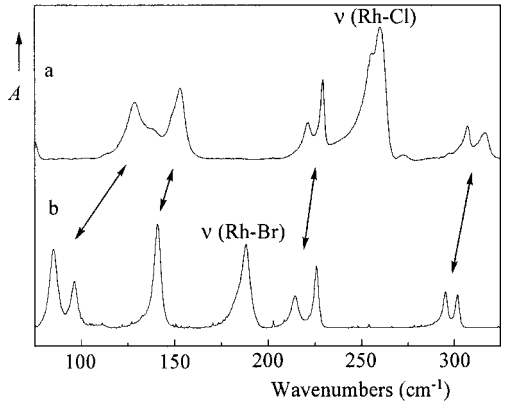

Figure 9. Far-IR spectra of complexes **1** (a) and **2** (b) dispersed in Nujol

square-planar arrangement. Only orbital contributions above 4% are incorporated in Table 3.

Table 3. Characteristics and one-electron energies of the HOMO-8 to LUMO+5 levels of [Rh(X)(tpy)] (**1**: X = Cl; **2**: X = Br), as calculated by the ADF/BP program; both complexes lie in the $x-y$ plane, and the Rh−X bond along the x-axis

MO	X	Energy (eV)	Terpyridine	Rh	X
Unoccupied orbitals					
$24a_1$	Cl	−1.170	31.3% ($18a_1$)	55.5% ($d_{x^2-y^2}$)	9.0% (p_x)
$26a_1$	Br	−1.350	30.2% ($18a_1$)	54.3% ($d_{x^2-y^2}$)	9.3% (p_x)
$11b_2$	Cl	−1.463	95.9% ($8b_2$)	−	−
$12b_2$	Br	−1.490	95.9% ($8b_2$)	−	−
$7a_2$	Cl	−2.057	92.1% ($6a_2$)	8.0% (d_{yz})	−
$8a_2$	Br	−2.084	92.2% ($6a_2$)	7.8% (d_{yz})	−
$10b_2$	Cl	−2.131	96.7% ($7b_2$)	−	−
$11b_2$	Br	−2.149	96.6% ($7b_2$)	−	−
$6a_2$	Cl	−2.998	95.8% ($5a_2$)	−	−
$7a_2$	Br	−3.026	95.7% ($5a_2$)	−	−
$9b_2$	Cl	−3.079	75.4% ($6b_2$)	18.3% (d_{xz})	−
$10b_2$	Br	−3.115	76.0% ($6b_2$)	17.6% (d_{xz})	−
Occupied orbitals					
$23a_1$	Cl	−4.119	−	77.6% (d_{z^2})	−
$25a_1$	Br	−4.129	−	78.0% (d_{z^2})	−
$19b_1$	Cl	−4.514	−	56.0% (d_{xy})	34.3% (p_y)
$20b_1$	Br	−4.500	−	49.6% (d_{xy})	41.1% (p_y)
$8b_2$	Cl	−4.519	26.3% (diff. b_2)	46.7% (d_{xz})	23.7% (p_z)
$9b_2$	Br	−4.501	24.6% (diff. b_2)	42.5% (d_{xz})	29.7% (p_z)
$5a_2$	Cl	−4.706	19.1% (diff. a_2)	77.5% (d_{yz})	−
$6a_2$	Br	−4.712	21.0% (diff. a_2)	77.9% (d_{yz})	−
$7b_2$	Cl	−6.105	−	22.4% (d_{xz})	70.0% (p_z)
$8b_2$	Br	−5.842	−	28.1% (d_{xz})	64.5% (p_z)
$18b_1$	Cl	−6.241	−	28.3% (d_{xy})	61.0% (p_y)
19b1	Br	−5.989	−	34.3% (d_{xy})	54.7% (p_y)
$4a_2$	Cl	−6.398	96.3% ($4a_2$)	−	−
$5a_2$	Br	−6.417	96.4% ($5a_2$)	−	−
$22a_1$	Cl	−6.602	10.6% ($18a_1$)	4.3% ($d_{x^2-y^2}$, s)	76.4% (p_x)
$24a_1$	Br	−6.327	9.2% ($18a_1$)	4.6% ($d_{x^2-y^2}$, s)	79.0% (p_x)
$6b_2$	Cl	−7.099	77.7% ($5b_2$)	−	−
$7b_2$	Br	−7.111	79.5% ($7b_2$)	−	−

The DFT calculations prove that variation of the ligand X (Cl and Br for complexes **1** and **2**, respectively) produces only small differences in orbital characters and energies

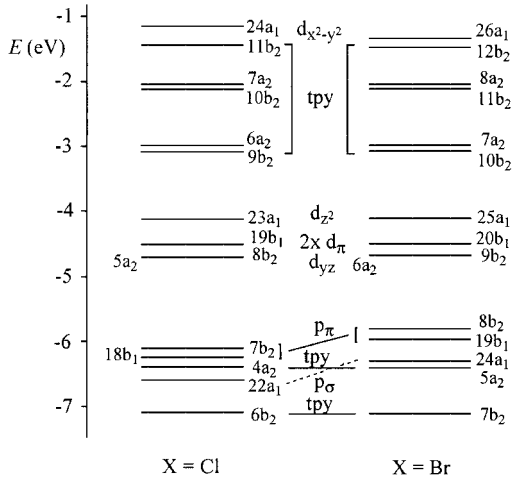

Figure 10. Relevant part of the MO diagrams of [Rh(X)(tpy)] (**1**: X = Cl; **2**: X = Br), as calculated with the ADF/BP program

(Table 3 and Figure 10). MO diagrams of complexes **1** and **2** clearly show that the comparable, predominantly Rh(d), orbitals of **1** and **2** (HOMO-1, -2, -3) have the same energies (except for empty $d_{x^2-y^2}$), which is also the case for the tpy-centred orbitals. Thus, the only comparable orbitals of **1** and **2** differing in energy are those with a predominant halide (p_π and p_σ) character (Figure 10). The variation of X in complexes **1** and **2** is reflected in the HOMO-4, HOMO-5 and HOMO-7 (X = Cl)/HOMO-6 (X = Br). These largely halide-based orbitals are ca. 0.3 eV lower in energy for complex **1** (X = Cl) than for **2** (X = Br).

According to the DFT calculations, the HOMO-1, HOMO-4 and HOMO-5 of **1** and **2** have significantly mixed X(p_π)/Rh(d_π) characters. Also, HOMO-2 of **1** and **2** is strongly mixed, tpy(π^*)/X(p_π)/Rh(d_π). In contrast, the HOMO and HOMO-3 of **1** and **2** are largely Rh(d_{z^2}) and Rh(d_{yz}), respectively, while HOMO-7 (X = Cl)/HOMO-6 (X = Br) has a predominantly halide (p_σ) character. As expected, the LUMO of **1** and **2** reside on the π^*(tpy) system, with some Rh(d_π) contribution. The higher-lying virtual orbitals of **1** and **2** are also almost exclusively localised on the π^*(tpy) system, except for LUMO+5, which is mainly Rh($d_{x^2-y^2}$).

Relevant electronic transitions (transition energies, wavelengths, oscillator strengths) of complexes **1** and **2** and their characters obtained from TD-DFT calculations are presented in Table 4 and Table 5, respectively. Apart from the first three excitations, only electronic transitions with oscillator strengths >0.015 have been incorporated.

The first seven single-electron transitions in Tables 4 and 5 are the same excitations from the comparable Rh(d) orbitals of complexes **1** and **2**. Single-electron transitions at higher energies are less similar owing to different characters of the molecular orbitals involved.

Experimental UV/Vis spectra and calculated electronic transitions for complexes **1** and **2** are shown in Figure 11 and Figure 12, respectively. The lowest seven single-electron transitions are highlighted, except for the forbidden transitions 1 of very low oscillator strengths.

Table 4. Single-electron transitions of complex **1**, as calculated with the ADF/BP program

Transition		Energy (eV)	Wavelength (nm)	Oscillator strength	Character
1	$23a_1 \rightarrow 9b_2$ (1.00)	1.142	1086	0.0002	MLCT
2	$8b_2 \rightarrow 6a_2$ (0.80) $5a_2 \rightarrow 9b_2$ (0.20)	1.605	773	0.0051	MLCT/XLCT
3	$5a_2 \rightarrow 6a_2$ (0.64) $8b_2 \rightarrow 9b_2$ (0.35)	1.753	707	0.0009	MLCT
4	$5a_2 \rightarrow 9b_2$ (0.77) $8b_2 \rightarrow 6a_2$ (0.18)	1.872	662	0.0437	MLCT
5	$8b_2 \rightarrow 9b_2$ (0.49) $5a_2 \rightarrow 6a_2$ (0.28)	2.075	597	0.0327	MLCT/XLCT
6	$8b_2 \rightarrow 10b_2$ (0.89) $8b_2 \rightarrow 11b_2$ (0.03)	2.494	497	0.0194	MLCT/XLCT
7	$5a_2 \rightarrow 10b_2$ (0.81) $8b_2 \rightarrow 7a_2$ (0.09)	2.760	449	0.1018	MLCT
8	$8b_2 \rightarrow 11b_2$ (0.56) $7b_2 \rightarrow 9b_2$ (0.35)	3.242	382	0.0478	MLCT/XLCT
9	$4a_2 \rightarrow 9b_2$ (0.64) $19b_1 \rightarrow 24a_1$(0.16)	3.628	342	0.2444	intraligand
10	$4a_2 \rightarrow 6a_2$ (0.56) $6b_2 \rightarrow 9b_2$ (0.25)	3.898	318	0.0535	intraligand
11	$6b_2 \rightarrow 6a_2$ (0.51) $4a_2 \rightarrow 10b_2$ (0.31)	4.327	287	0.1278	intraligand
12	$4a_2 \rightarrow 7a_2$ (0.41) $6b_2 \rightarrow 9b_2$ (0.28)	4.396	282	0.0549	intraligand
13	$4a_2 \rightarrow 10b_2$ (0.54) $6b_2 \rightarrow 6a_2$ (0.27)	4.546	273	0.2673	intraligand
14	$4a_2 \rightarrow 7a_2$ (0.37) $6b_2 \rightarrow 9b_2$ (0.20)	4.558	272	0.0545	intraligand

Table 5. Single-electron transitions of complex **2**, as calculated with the ADF/BP program

Transition		Energy (eV)	Wavelength (nm)	Oscillator strength	Character
1	$25a_1 \rightarrow 10b_2$ (1.00)	1.112	1115	0.0002	MLCT
2	$9b_2 \rightarrow 7a_2$ (0.83) $6a_2 \rightarrow 10b_2$ (0.17)	1.556	795	0.0057	MLCT/XLCT
3	$6a_2 \rightarrow 7a_2$ (0.57) $9b_2 \rightarrow 10b_2$ (0.42)	1.713	724	0.0036	MLCT/XLCT
4	$6a_2 \rightarrow 10b_2$ (0.80) $9b_2 \rightarrow 7a_2$ (0.16)	1.831	677	0.0401	MLCT
5	$9b_2 \rightarrow 10b_2$ (0.44) $6a_2 \rightarrow 7a_2$ (0.35)	2.016	615	0.0411	MLCT/XLCT
6	$9b_2 \rightarrow 11b_2$ (0.91) $9b_2 \rightarrow 12b_2$ (0.03)	2.448	507	0.0205	MLCT/XLCT
7	$6a_2 \rightarrow 11b_2$ (0.82) $9b_2 \rightarrow 8a_2$ (0.06)	2.733	454	0.0830	MLCT
8	$8b_2 \rightarrow 10b_2$ (0.58) $6a_2 \rightarrow 8a_2$ (0.35)	2.893	429	0.0229	XLCT/MLCT
9	$6a_2 \rightarrow 8a_2$ (0.28) $8b_2 \rightarrow 10b_2$(0.19)	3.488	356	0.0285	MLCT/XLCT
10	$5a_2 \rightarrow 10b_2$ (0.76) $7b_2 \rightarrow 7a_2$ (0.08)	3.587	346	0.2229	intraligand
11	$5a_2 \rightarrow 7a_2$ (0.58) $7b_2 \rightarrow 10b_2$ (0.24)	3.882	319	0.0506	intraligand
12	$7b_2 \rightarrow 7a_2$ (0.55) $5a_2 \rightarrow 11b_2$ (0.29)	4.314	287	0.1409	intraligand
13	$8b_2 \rightarrow 12b_2$ (0.37) $7b_2 \rightarrow 10b_2$ (0.31)	4.329	286	0.0218	intraligand
14	$5a_2 \rightarrow 11b_2$ (0.57) $7b_2 \rightarrow 7a_2$ (0.24)	4.538	273	0.2338	intraligand

Assignment of the absorption bands in the UV/Visible region (250−900 nm) is facilitated by the TD-DFT calculations. The calculated electronic transitions of complex **1** match fairly well the experimental electronic absorption spectrum, except for transition 7 (Table 4). For complex **2** the deviations in the UV region are larger. The intense ab-

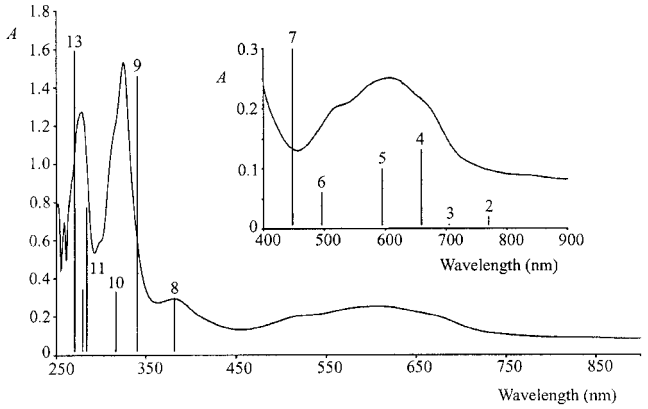

Figure 11. Electronic absorption spectrum of complex **1** (7.27×10^{-5} M) in EtOH. Major electronic transitions of complex **1**, as calculated by the ADF/BP method (Table 4)

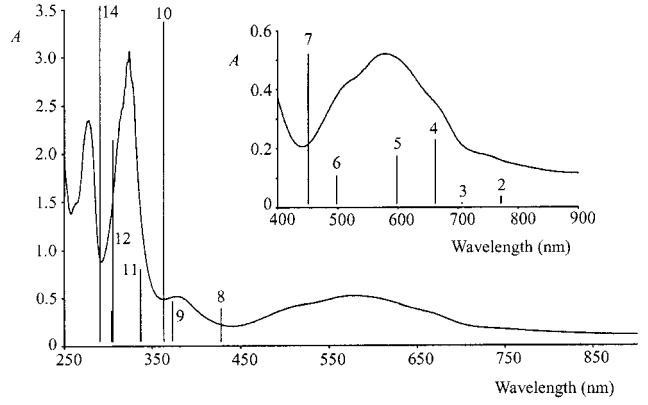

Figure 12. Electronic absorption spectrum of complex **2** (1.36×10^{-4} M) in EtOH. Major electronic transitions of complex **2**, as calculated by the ADF/BP method (Table 5)

sorption bands in the region 250−350 nm are predominantly due to intraligand tpy transitions. The pronounced composed absorption band in the 450−700 nm region encompasses mixed MLCT/XLCT (6, 5) and MLCT (4) transitions. Minor absorption bands in the region 700−900 nm belong to symmetry-forbidden (in a perfect square-planar coordination) MLCT (3), MLCT/XLCT (2) and MLCT (1; HOMO-to-LUMO) transitions.

Cyclic Voltammetry of Complexes 1 and 2

Solutions of complexes **1** and **2** in dry DMF, freshly prepared under an argon atmosphere, show very similar cyclic voltammograms. Therefore, only the cyclic voltammogram of complex **1** is depicted in Figure 13.

Electrochemical oxidation of complexes **1** and **2** is partly chemically reversible on the cyclic voltammetry time scale (ν = 100 mV s^{-1}) at room temperature (Figure 13). In accordance with DFT results (Table 3), this anodic process corresponds to a one-electron oxidation of the formal Rh^I centre to the corresponding Rh^{II} product. Further oxidation of $\mathbf{1}^+$ and $\mathbf{2}^+$ to the corresponding Rh^{III} species was not observed. The oxidation potentials of **1** and **2** show

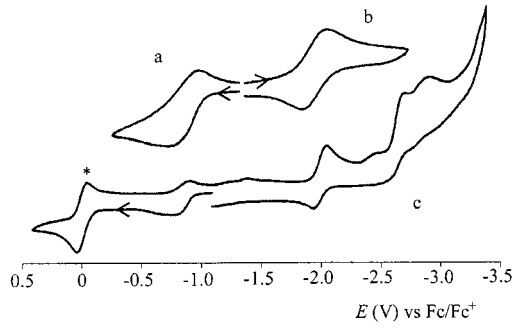

Figure 13. Cyclic voltammogram of complex **1** in DMF at a Pt disk electrode, ν = 100 mV s^{-1}: (a) Partly reversible one-electron oxidation of the Rh^I centre to Rh^{II} at T = 293 K; (b) reversible one-electron reduction of the tpy ligand at T = 233 K; (c) complete cyclic voltammogram at T = 293 K. Asterisk denotes the Fc/Fc^+ redox couple

negligible differences: $E_{1/2}$ (**1**) = −0.84 V vs. Fc/Fc^+; $E_{1/2}$ (**2**) = −0.83 V vs. Fc/Fc^+. This agrees with the DFT-calculated energies of the HOMO for both complexes, which differ merely by 0.01 eV (Table 3).

Electrochemical reduction of **1** and **2** is fully reversible on the cyclic voltammetry time scale at T = 233 K (ν = 100 mV s^{-1}) (Figure 13), being predominantly localised on the lowest π*(tpy) level (Table 3). Understandably, therefore, the reduction potentials of both complexes are nearly identical ($E_{1/2}$ (**1**) = −1.98 V and $E_{1/2}$ (**2**) = −1.97 V vs. Fc/Fc^+). The calculated LUMO energies of **1** and **2** differ to a slightly greater extent (0.036 eV).

Discussion

Syntheses of Complexes 1−4

Under the right reaction conditions, in particular with a suitable solvent, the studied Rh^I-terpyridine complexes are fairly simply synthesised, in nearly quantitative yields. The dark blue Rh^I-terpyridine products are highly air-sensitive and readily oxidise to yellow/red Rh^{III} species.

Having prepared complex **1** in toluene and washed it subsequently with hot THF, crystals were grown during gentle cooling of the combined THF phases. However, this method was unsuccessful for the crystallisation of the other studied Rh^I-terpyridine complexes. In contrast to complex **1**, complex **2** could not be synthesised in toluene; instead, only orange Rh^{III} species were formed. Complex **2** was only obtained in EtOH. Similar to complex **1**, complex **3** could be prepared in various organic solvents such as benzene, THF, Et_2O and EtOH. Attempts to synthesise the Rh−Br complex analogous to **3** only gave red oxidised products. Finally, despite the instability of the carboranyl-tpy unit in various organic solvents, complex **4** was stable for several weeks in EtOH and crystallised upon standing at room temperature.

X-ray Crystallographic Studies of Complexes 1 and 4

In contrast to the fairly facile syntheses of the studied Rh^I-terpyridine complexes, their characterisation is compli-

cated by their low solubility in organic solvents. The crystal packing of various square-planar d^8 transition metal complexes containing rigid aromatic ligands is dominated by π−π stacking interactions,[21−23] leading to poor solubility and so hampering full characterisation. The distance between the sheets (3.508 Å) in the crystal of **1** is due to this type of π-stacking (Figure 3 and Figure 4).

Complex **4**, bearing the bulky carboranyl group,[24] was prepared to prevent such π-stacking. In the crystal, molecules of **4** are packed in discrete dimers with a Rh−Rh′ distance of 3.1503(13) Å, which is too long for a single bond but rather short for a non-bonding contact.[25] Clearly, the carboranyl group has resulted in a structure without strong π-stacking, the dimeric structure being apparently the highest degree of association possible with this ligand. Unfortunately, even this non-π-stacked complex does not dissolve well in organic solvents. Thus, preventing π-stacking is not a sufficient condition for increased solubility of Rh^I-terpyridine complexes.

Despite the dramatic difference in the packing of complexes **1** and **4**, the coordination geometries of the mononuclear units are very similar, and similar to isoelectronic Pd^{II} [26] and Pt^{II} [27] terpyridine complexes. The corresponding bond lengths (Table 1) and angles (Table 2) are almost the same. Rh−N distances for both **1** and **4** [1.891(6)−2.026(7) Å] are significantly shorter than (κ^1) Rh^{II}-terpyridine,[12] (κ^3) Rh^{II}-terpyridine[12] and (κ^3) Rh^I-diiminepyridine[6] complexes. For Rh^I-chloride complexes with the diiminepyridine ligands 2,6-bis(R^2-iminomethyl)pyridine and 2,6-bis(R^2-iminoethyl)pyridine (R^2 = *i*Pr, *t*Bu), Haarman et al. have shown that the angle between the N−N−N plane and the Rh−Cl axis is a useful measure of steric interactions between the R^2 groups and the chlorine atom.[6] In our study, these angles are 0.25(7)° for **1** and 3.4(3)° for **4**, which are much smaller than those found by Haarman et al. [5.34(16)−11.73(11)°]. We therefore conclude that steric interactions between the terpyridine ligand and the chlorine atom in complexes **1** and **4** are not significant.

FIR Spectra of Complexes 1 and 2

The Rh^I(X)-terpyridine complexes contain only a single Rh−X bond. This facilitates the analysis of their far-IR (FIR) spectra compared with those of $Rh^{III}(X)_3$-tpy[20] species. Assignment of ν(Rh−X) for **1** (256−260 cm^{-1}) and **2** (188 cm^{-1}) is straightforward. Bands at 129−138 cm^{-1} (**1**) and 85−96 cm^{-1} (**2**) are tentatively assigned to Rh−X bending vibrations. The influence of the Rh-metal oxidation state and of the absence/presence of axial halides on the ν(Rh−X) modes for Rh^I(X)-tpy and $Rh^{III}(X)_3$-tpy has not been thoroughly studied. Rh^I−X bonds are generally weaker than Rh^{III}−X bonds, due to stronger π-donation from X to Rh^{III} than to Rh^I metal ions. Therefore, the larger ν(Rh−X) wavenumbers reported for [$Rh(Cl)_3$(tpy)] (330−380 cm^{-1}) and [$Rh(Br)_3$(tpy)] (205−209 cm^{-1}) are reasonable.[20]

Bonding Properties of Complexes 1 and 2

The experimental and corresponding DFT calculated bond lengths and angles in complexes **1** and **2** (Table 1 and Table 2) are in good agreement. This confirms that the used GGA functional (Becke−Perdew), for geometry determination, and the chosen basis set for the DFT calculations, run by the ADF program, are adequate.

From the DFT calculations, the HOMO of complexes **1** and **2** is clearly located mainly on the Rh(d_{z^2}) orbital. This property, combined with the strong electron-donating nitrogen atoms coordinated at the Rh^I centre, makes complexes **1** and **2** extremely nucleophilic and, thereby, very reactive towards, e.g., oxygen and carbon−halogen bonds.[28] While the HOMO of **1** and **2** has a strong metal character, the LUMO is predominantly located on the π* system of the tpy ligand. The HOMO-1 and HOMO-2 can be characterised as antibonding combinations (π-interactions) of p(X) (X = Cl, Br) and d(Rh) orbitals. Both molecular orbitals are destabilised compared with the HOMO-3 that is mainly Rh(d_{yz}). HOMO-4 and HOMO-5 are bonding orbitals − π-interactions between p_π(X) and d_π(Rh) orbitals. HOMO-6 (X = Cl)/HOMO-7 (X = Br) have exclusively a ligand tpy character (like the HOMO-8). HOMO-7 (X = Cl)/HOMO-6 (X = Br) have predominantly a halide character (σ-interaction).

Complexes **1** and **2** feature comparable electronic transitions from orbitals of the same character (Table 4 and Table 5). The lowest seven excitations in both complexes correspond mutually very well. At higher energies, there is no longer a one-to-one relationship between the composition of the excited states of the Cl and Br complexes (**1** and **2**, respectively) in terms of one-electron transitions. After the seventh excitation, the Br p-orbitals play a more dominant role in the single-electron transitions for complex **2** than the Cl p-orbitals for complex **1**. This is mainly due to the difference in energy of the halide p-orbitals (Figure 10).

Regarding differences, for complex **2** an extra electronic transition (viz. 9, Table 5) has been calculated by the ADF/BP program, which has no counterpart in complex **1**. Furthermore, for complex **1**, the electronic transition 8 has a predominant MLCT character (Table 4), while the corresponding electronic transition 8 in complex **2** can better be assigned as XLCT (Table 5).

The MO diagrams of complexes **1** and **2** are very similar. Only the unoccupied predominantly Rh($d_{x^2-y^2}$) and occupied halide molecular orbitals of **1** and **2**, viz. LUMO+5, HOMO-4, HOMO-5 and HOMO-7 (X = Cl)/HOMO-6 (X = Br), slightly differ in energies (ca. 0.3 eV), as displayed by their molecular orbital diagrams in Figure 10. This rationalises the similar UV/Vis spectra and cyclic voltammograms of complexes **1** and **2**. Assignment of the UV/Vis absorption bands of **1** and **2** to particular types of electronic transitions is facilitated by the TD-DFT calculations. The most intense absorption bands in the UV region 250−350 nm are solely assigned as intraligand tpy transitions. The dominant and minor absorption bands and shoulders in the visible region 450−900 nm belong to mixed

electronic transitions that vary in nature from pure MLCT to mixed XLCT/MLCT charge transfers (Tables 4 and 5). The HOMO−LUMO transition is not symmetry allowed (Table 3), resulting in a very low oscillator strength (Tables 4 and 5). Exclusive Rh-centred (d−d, LF) transitions are not observed. The only notable d−d contribution, of limited significance (16% to transition 9) has been calculated for complex **1** (Table 4).

Complexes **1** and **2** have fairly negative oxidation potentials, strongly indicating that the Rh^I metal centres indeed accommodate high electron densities. The one-electron oxidation of formally Rh^I to Rh^{II} at room temperature is partly reversible on the time scale of seconds. The relative stability of the Rh^{II} species can be ascribed to the high electron-donating capacity of the coordinated tpy and halide ligands. Notably, the subsequent oxidation of Rh^{II} to Rh^{III} was not observed in the available potential window.

At room temperature, the initial one-electron reduction of complexes **1** and **2** in DMF is also partly chemically reversible. A fully reversible scan (ν = 100 mV/s) was achieved at T = 233 K. Long lifetimes of radical anions of **1** and **2** result from the accommodation of the added electron in the π*(tpy) LUMO, as evidenced by the DFT calculations. The subsequent thermal reaction of the radical anions most likely involves release of the halide ligand to compensate for the high electron density at the metal centre. Slow halide dissociation also occurs with the radical anion of the much less electron-rich complex [RhCl(CO)(*i*Pr_2Ph-BIAN)] [*i*Pr_2Ph-BIAN = *N*,*N*′-1,2-bis(2,6-diisopropylphenylimino)acenaphthene].[29,30]

Conclusions

We report the first successful syntheses, characterisation and determination of properties of neutral rigid square-planar Rh^I-terpyridine complexes **1**−**4**. For the syntheses, an appropriate solvent is of crucial importance for each complex. Characterisation is difficult, primarily due to the low solubility (formation of π-stacked aggregates and discrete dimers) and high reactivity of the complexes, promoted by the high electron density on the Rh centre. The Rh^I-terpyridine complexes show no steric repulsion between the halides and the tpy ligand, as evidenced by the crystal structures. Variation of the halide ligand in complexes **1** and **2** (Cl and Br, respectively) has no significant influence on the electronic structure. Their HOMO is predominantly localised on the Rh^I centre (d_{z^2}), and the LUMO resides on the tpy ligand.

Experimental Section

General Remarks: The syntheses of the Rh^I-terpyridine complexes under study and all manipulations with them were strictly performed under an inert atmosphere of purified dry argon or nitrogen, using standard Schlenk techniques. Solvents and reagents were dried and purified by standard procedures.[31] ^{1}H NMR measurements were carried out at 294 K with a Bruker AMX 300 spectrometer operating at 300 MHz. Fast Atom Bombardment (FAB^+) mass spectra were obtained with a JEOL JMS SX/SX102A four-sector mass spectrometer, coupled to a JEOL MS-7000 data system. Samples were loaded in a matrix phase (glycerol) on a stainless steel probe and bombarded with xenon atoms (3 keV). During the high-resolution FAB MS measurements a resolving power of 5000 (10% valley definition) was used. CsI and glycerol served as calibration standards. Elemental analyses were performed by H. Kolbe Mikroanalytisches Laboratorium (Mülheim an der Ruhr, Germany) and Analytische Laboratorien GmbH (Lindlar, Germany).

The tpy and 4′-chloro-2,2′:6′,2′′-terpyridine (4′-Cl-tpy) ligands are commercially available (Aldrich). Precursor complexes $[Rh(X)(COD)]_2$ (X = Cl, Br; COD = cycloocta-1,5-diene)[32] and the ligand 4′-(*tert*-butyldimethylsilyl-*o*-carboranyl)-2,2′:6′,2′′-terpyridine (carboranyl-tpy)[33] were synthesised according to literature procedures.

[Rh(Cl)(Tpy)] (1): Solutions of tpy (1.0 g, 4.3 mmol) and $[Rh(Cl)(COD)]_2$ (1.0 g, 2.0 mmol) in toluene (50 mL) were mixed and stirred together at room temperature. After five minutes, a dark blue precipitate of complex **1** was formed. The product was filtered off, washed with hot THF (3×20 mL) and dried under reduced pressure. Yield 0.7 g (95%). Gentle cooling of the collected THF phases afforded needle-shaped dark blue crystals suitable for X-ray diffraction studies. A small portion of the solid was recrystallised from hot benzonitrile as dark blue leaflets that were used for elemental analysis. FAB^+ MS: *m*/*z* = 371.98 [M^+]. $C_{15}H_{11}ClN_3Rh$ (370.97): calcd. C 48.48, H 2.98, Cl 9.54, N 11.31; found C 48.60, H 3.04, Cl 9.80, N 11.43.

[Rh(Br)(tpy)] (2): A solution of tpy (0.024 g, 0.10 mmol) and $[Rh(Br)(COD)]_2$ (0.03 g, 0.05 mmol) in EtOH (20 mL) was stirred at room temperature for 5 to 10 min, having afforded a dark blue suspension. After filtration, the so-obtained dark blue solid was washed with EtOH (3×10 mL), followed by pentane (3×10 mL). The product was then dried under reduced pressure. Complex **2** was collected as a dark blue powder in nearly quantitative yield (20 mg). FAB^+ MS: *m*/*z* = 414.92 [M^+]. $C_{15}H_{11}BrN_3Rh$ (414.92): calcd. C 43.30, H 2.66, Br 19.20, N 10.10; found C 43.28, H 2.66, Br 19.32, N 10.06.

[Rh(Cl)(4′-Cl-tpy)] (3): Solutions of 4′-Cl-tpy (0.045 g, 0.17 mmol) and $[Rh(Cl)(COD)]_2$ (0.04 g, 0.08 mmol) in toluene (10 mL) were mixed at room temperature. After stirring for 5 to 10 min, a dark blue solid precipitated that was filtered off, washed with toluene (3×10 mL), pentane (3×10 mL), and dried under reduced pressure. Complex **3** was collected as a dark blue powder in nearly quantitative yield (32 mg). FAB^+ MS: *m*/*z* = 404.93 [M^+]. $C_{15}H_{10}Cl_2N_3Rh$ (404.93): calcd. C 44.37, H 2.48, Cl 17.46, N 10.35; found C 44.26, H 2.55, Cl 17.55, N 10.18.

[Rh(Cl)(carboranyl-tpy)] (4): A solution of carboranyl-tpy (0.2 g, 0.41 mmol) and $[RhCl(COD)]_2$ (0.1 g, 0.20 mmol) in EtOH (100 mL) was stirred for 6 h at room temperature. After standing for three weeks and decanting the dark purple supernatant liquid, dark blue crystals of **4** were collected. Yield 0.11 g (90%). ^{1}H NMR (300 MHz, C_6D_6, 20 °C): δ (ppm) = 7.38 (s, 2 H), 7.09 [t, $^3J_{H,H}$ = 8 Hz, 2 H, C(5,5′′)−H], 6.94 [d, $^3J_{H,H}$ = 8 Hz, 2 H, C(3,3′′)−H], 6.84 [t, $^3J_{H,H}$ = 7 Hz, 2 H, C(4,4′′)−H], 0.65 (s, *t*Bu), −0.43 [s, −Si(Me)$_2$−]. $C_{23}H_{35}B_{10}ClN_3SiRh{\cdot}CH_3CH_2OH$ (675.27): calcd. C 44.54, H 6.13, N 6.23; found C 44.32, H 6.03, N 6.31.

Complexes **1** and **3** could also be synthesised in organic solvents other than toluene, such as benzene, THF, Et_2O and EtOH. In contrast, the syntheses of complexes **2** and **4** were only successful

in EtOH. Complexes **1**−**4** react rapidly with MeOH to produce unidentified red Rh^{III} species.

X-ray Structure Determination of Complexes 1 and 4: A dark blue single crystal was mounted on a capillary. Intensity data were collected at room temperature with an Enraf-Nonius CAD4 diffractometer, using the ω-2θ scan mode. Unit cell dimensions were determined from the angular setting of 25 reflections. Intensity data were corrected for Lorentz and polarisation effects. A semi-empirical absorption correction (ψ-scans)[34] was applied. The structures were solved by the program system DIRDIF,[35] using the program PATTY[36] to locate the rhodium atom, and refined with standard methods (refinement against F^2 of all reflections with SHELXL-97[37]), with anisotropic parameters for the non-hydrogen atoms. All hydrogen atoms were placed at calculated positions and refined riding on the parent atoms. A structure determination summary is presented in Table 6. PLATON[38] drawings of complexes **1** and **4** are shown in Figures 2 and 6, respectively. Selected bond lengths and angles for both crystal structures are given in Tables 1 and 2. CCDC-125107 (for **1**) and -125106 (for **4**) contain the supplementary crystallographic data for this paper. These data can be obtained free of charge at www.ccdc.cam.ac.uk/conts/retrieving.html [or from the Cambridge Crystallographic Data Centre, 12 Union Road, Cambridge CB2 1EZ, UK; Fax: (internat.) +44-1223-336-033; E-mail: deposit@ccdc.cam.ac.uk].

UV/Vis and FIR Spectra of Complexes 1 and 2: Electronic absorption spectra were measured with a HP 8453 diode-array spectrophotometer. Far-infrared (FIR) spectra were recorded between 75 and 375 cm^{-1} with a BOMEM DA3.02 FTIR spectrometer, using a polyethylene cell filled under an argon atmosphere. All FIR experiments used a globar light source and a helium-cooled germanium bolometer operating at 4.2 K. The spectra (128 scans) were recorded at 0.5 cm^{-1} resolution. Samples were dispersed in Nujol under an argon atmosphere.

Density Functional Theoretical (DFT) Study of Complexes 1 and 2: Density functional theory (DFT) was employed to determine the ground-state electronic structures of complexes **1** and **2**, and time-dependent density functional theory (TD-DFT) to describe the corresponding electronic transitions.[39−41] It is important to stress that the Kohn−Shan molecular orbitals, arising from DFT calculations, are physically meaningful,[42,43] and that the accuracy of excitation energies determined with TD-DFT is often similar to that of the most advanced ab initio methods.[44,45]

Calculations of geometry-optimised [Rh(Cl)(tpy)] (**1′**) and [Rh(Br)(tpy)] (**2′**) were performed with the Amsterdam Density Functional (ADF) program.[46] Crystallographic data of complex **1** were used to provide an initial estimate of the equilibrium geometry. Atomic coordinates were then projected onto a plane, and geometry optimisation was performed for the ground state. A separate optimisation was carried out for each molecule, with constrained planar geometry and C_{2v} symmetry.

For all calculations, including the geometry optimisation, the following basis sets were employed: for C, N, H, Cl and Br, an uncontracted triple-ζ Slater-type orbital (STO) basis with two polarisation functions; for Rh, an uncontracted triple-ζ STO basis with one polarisation function (5p). Core orbitals were frozen for C and N (1s), Cl (2s, 2p), Br (3s, 3p), and Rh (1s-3d).

Table 6. Crystallographic data and summary of the refinement for complexes **1** and **4**

Complex	**1**	**4**
Crystal colour	dark blue	dark blue
Crystal shape	irregular rod	plate
Crystal size, mm	0.41 × 0.19 × 0.12	0.38 × 0.30 × 0.05
Empirical formula	$C_{15}H_{11}ClN_3Rh$	$C_{23}H_{35}B_{10}ClN_3RhSi{\cdot}0.7\ C_2H_5OH$
M_w	371.63	660.34
T, K	293(2)	200
Radiation	Cu-K_α (graphite monochromator)	Mo-K_α (graphite monochromator)
Wavelength, Å	1.54184	0.71073
Crystal system	monoclinic	monoclinic
Space group	$P2_1/n$	$P2_1/c$
Unit cell dimensions	a = 9.5594(5) Å	a = 20.5101(15) Å
	b = 11.1190(5) Å, β= 107.936(4)°	b = 10.5314(11) Å, β= 99.674(8)°
	c = 13.0679(5) Å	c = 15.0070(15) Å
V, Å^3	1321.49(10)	3195.4(5)
Z	4	4
$D_{calcd.}$, g cm^{-3}	1.868	1.373
μ, mm^{-1}	12.233	0.68
F(000)	736	1353
Θ range for data collection, °	5.06 to 69.91	1.01 to 27.47
Index ranges	$0 \le h \le 11$, $-13 \le k \le 13$, $-15 \le l \le 15$	$-26 \le h \le 26$, $0 \le k \le 13$, $-19 \le l \le 13$
Reflections collected/unique	5096/2495 [R_{int} = 0.1058][a]	9900/7321 [R_{int} = 0.0568][a]
Reflections observed	1743 ([$I_o > 2\sigma(I_o)$])	3702 ([$I_o > 2\sigma(I_o)$])
Range of relat. transm. factors	1.463 and 0.77	0.98 and 0.93
Data/restraints/parameters	2495/0/181	7321/14/388
Goodness-of-fit on F^2	1.059	1.025
Final R indices [$I > 2\sigma(I)$][b] [c]	R_1 = 0.0569, wR_2 = 0.1465	R_1 = 0.0791, wR_2 = 0.1528
R indices (all data)	R_1 = 0.0888, wR_2 = 0.1638	R_1 = 0.1809, wR_2 = 0.1986
Diff. peak/hole, e·Å^{-3}	1.321/−1.142	0.92/−0.93

[a] $R_{int} = \Sigma|F_o^2 - F_o^2(\text{mean})|/\Sigma F_o^2$. [b] Unweighted agreement factor $R_1 = \Sigma||F_o| - |F_c||/\Sigma|F_o|$. [c] The weighted agreement factor $wR_2 = [\Sigma[w||F_o| - |F_c||^2/\Sigma w|F_o|^2]^{1/2}$, where $w = 4F^2/\sigma^2(F^2)$.

To approximate the exchange-correlation potential, the generalised gradient approximation (GGA) was adopted, which employs the Becke gradient approximation for the exchange,[47] and Perdew approximation for correlation (ADF/BP).[48] After the geometry optimisation, calculations were performed for three different fragments of each complex molecule; the tpy ligand, Cl/Br and Rh. The ADF package allows the results of the fragment calculations to be used in ground-state calculations of each complete molecule, and the molecular orbitals (MOs) to be analysed in terms of the fragments' orbitals. In all calculations, C_{2v} symmetry was incorporated for the terpyridine ligand and the entire molecule. For the individual-atom fragments, spherical symmetry was imposed.

The ADF-RESPONSE module,[49] an extension of the ADF, was used to perform TD-DFT calculations, for the ground-state optimised geometry. These calculations provide excitation energies and relative contributions of individual occupied-to-virtual MO transitions to each excitation.

Cyclic Voltammetry of Complexes 1 and 2: Cyclic voltammetry was performed in a gas-tight cell under an inert atmosphere of dry argon. The cell was equipped with a Pt disk working electrode (apparent surface area of 0.42 mm^2), Pt wire auxiliary electrode, and Ag wire pseudoreference electrode. Before each experiment, the working electrode was carefully polished with a 0.25 μm grain diamond paste. Redox potentials are reported against the ferrocene/ferrocenium (Fc/Fc^+) redox couple, used as an internal reference standard.[50] Cyclic voltammetric experiments were performed with complexes **1** and **2** (10^{-4} M) in dry HPLC-grade dimethylformamide (DMF). The potential was controlled with a PAR Model 283 potentiostat equipped with positive feedback for ohmic drop compensation.

Acknowledgments

Prof. Anton W. Gal and Dr. Peter H. M. Budzelaar (University of Nijmegen) are thanked for their interest in this work and for their help with the syntheses.

[1] E. C. Constable, *Adv. Inorg. Chem. Rad.* **1986**, *30*, 69−121.
[2] E. C. Constable, *Prog. Inorg. Chem.* **1994**, *42*, 67−138.
[3] R. E. Rülke, V. E. Kaasjager, P. Wehman, A. L. Spek, C. J. Elsevier, P. W. N. M. van Leeuwen, K. Vrieze, *Organometallics* **1996**, *15*, 668−677.
[4] K. Vrieze, J. H. Groen, J. G. P. Delis, C. J. Elsevier, P. W. N. M. van Leeuwen, *New J. Chem.* **1997**, *21*, 807−813.
[5] J. H. Groen, A. de Zwart, M. J. M. Vlaar, J. M. Ernsting, P. W. N. M. van Leeuwen, K. Vrieze, H. Kooijman, W. J. J. Smeets, A. L. Spek, P. H. M. Budzelaar, Q. Xiang, R. P. Thummel, *Eur. J. Inorg. Chem.* **1998**, 1129−1143.
[6] H. F. Haarman, J. M. Ernsting, M. Kranenburg, H. Kooijman, N. Veldman, A. L. Spek, P. W. N. M. van Leeuwen, K. Vrieze, *Organometallics* **1997**, *16*, 887−900.
[7] H. F. Haarman, F. R. Bregman, P. W. N. M. van Leeuwen, K. Vrieze, *Organometallics* **1997**, *16*, 979−985.
[8] H. F. Haarman, J. W. F. Kaagman, W. J. J. Smeets, A. L. Spek, K. Vrieze, *Inorg. Chim. Acta* **1998**, *270*, 34−45.
[9] H.-W. Frühauf, Habilitation Thesis, University of Duisburg, Germany, **1980**.
[10] G. T. Morgan, F. H. Bursthall, *J. Chem. Soc.* **1932**, 20−30.
[11] G. T. Morgan, F. H. Bursthall, *J. Chem. Soc.* **1937**, 1649−1655.
[12] F. P. Pruchnik, F. Robert, Y. Jeannin, S. Jeannin, *Inorg. Chem.* **1996**, *35*, 4261−4263.
[13] F. P. Pruchnik, P. Jakimowicz, Z. Ciunik, J. Zakrzewska-Czerwinska, A. Opolski, J. Wietrzyk, E. Wojdat, *Inorg. Chim. Acta* **2002**, *334*, 59−66.
[14] W. K. Seok, H. N. Lee, M. Y. Kim, T. M. Klapotke, Y. Dong, H. Yun, *J. Organomet. Chem.* **2002**, *654*, 170−175.
[15] T. Yutaka, I. Mori, M. Kurihara, J. Mizutani, K. Kubo, S. Furusho, K. Matsumura, N. Tamai, H. Nishihara, *Inorg. Chem.* **2001**, *40*, 4986−4995.
[16] M. Y. Kim, W. K. Seok, Y. Dong, H. Yun, *Inorg. Chim. Acta* **2001**, *319*, 194−198.
[17] F. Odobel, J. P. Sauvage, A. Harriman, *Tetrahedron Lett.* **1993**, *34*, 8113−8116.
[18] M. E. Frink, D. Steven, H. A. Goodwin, R. J. Watts, P. C. Ford, *Inorg. Chem.* **1988**, *27*, 1283−1286.
[19] R. Marcec, *React. Kinet. Catal. Lett.* **1986**, *31*, 337−341.
[20] I. I. Bhayat, W. R. McWhinnie, *Spectrochim. Acta Part A* **1972**, *28*, 743−751.
[21] G. R. Cayley, D. W. Margerum, *J. Chem. Soc., Chem. Commun.* **1974**, 1002−1004.
[22] M. Chou, C. Creutz, D. Mahajan, N. Sutin, A. P. Zipp, *Inorg. Chem.* **1982**, *21*, 3989−3997.
[23] G. Arena, L. M. Scolaro, R. F. Pasternack, R. Romeo, *Inorg. Chem.* **1995**, *34*, 2994−3007.
[24] D. Armspach, E. C. Constable, C. E. Housecroft, M. Neuburger, M. Zehnder, *J. Organomet. Chem.* **1998**, *550*, 193−206.
[25] G. Aullón, P. Alemany, S. Alvarez, *Inorg. Chem.* **1996**, *35*, 5061−5067.
[26] G. M. Intille, C. E. Pfuger, W. A. Baker, *J. Cryst. Mol. Struct.* **1973**, *3*, 47−54.
[27] K. W. Jennette, J. T. Gill, J. A. Sadownick, S. J. Lippard, *J. Am. Chem. Soc.* **1976**, *98*, 6159−6168.
[28] B. C. de Pater, E. J. Zijp, H.-W. Frühauf, J. M. Ernsting, C. J. Elsevier, K. Vricze, P. H. M. Budzelaar, A. W. Gal, *Organometallics* **2004**, *23*, 269−279.
[29] E. Dova, K. Goubitz, A. van Langevelde, R. Driessen, T. Mahabiersing, R. Blaauw, R. Peschar, H. Schenk, *J. Synchrotron Rad.* **2001**, *8*, 1186−1190.
[30] T. Mahabiersing, H. Luyten, R. Nieuwendam, F. Hartl, *Collect. Czech. Chem. Commun.* **2003**, *68*, 1687−1709.
[31] D. D. Perrin, W. L. F. Armarego, *Purification of Laboratory Chemicals*, 3rd ed., Pergamon Press, Exeter, United Kingdom, **1988**.
[32] A. van der Ent, A. L. Onderdelinden, *Inorg. Synth.* **1990**, *28*, 90−92.
[33] D. Armspach, E. C. Constable, C. E. Housecroft, M. Neuburger, M. Zehnder, *New J. Chem.* **1996**, *20*, 331−335.
[34] A. C. T. North, D. C. Phillips, F. S. Mathews, *Acta Crystallogr., Sect. A* 1968, 24, 351−359.
[35] P. T. Beurskens, G. Beurskens, W. P. Bosman, R. de Gelder, S. Garcia-Granda, R. O. Gould, R. Istrael, J. M. M. Smits, *DIRDIF-96.* A computer program system for crystal structure determination by Patterson methods and direct methods applied to difference structure factors, Laboratory of Crystallography, University of Nijmegen, The Netherlands, **1996**.
[36] P. T. Beurskens, P. T. Admiraal, G. Behm, G. Beurskens, J. M. M. Smits, C. Smykalla, *Z. Kristallogr.* **1991**, Suppl. 4, 99.
[37] G. M. Sheldrick, *SHELXL-97*, Program for the refinement of crystal structures, University of Göttingen, Germany, **1997**.
[38] A. L. Spek, *PLATON, A Multipurpose Crystallographic Tool*, Utrecht University, Utrecht, The Netherlands, **2002**.
[39] M. Casida, *Recent Advances in Density Functional Methods*, World Scientific, Singapore, **1995**.
[40] E. K. U. Gross, W. Kohn, *Adv. Quantum Chem.* **1990**, *21*, 255−291.
[41] E. K. U. Gross, J. F. Dobson, M. Petersilka, *Density Functional Theory*, Springer, Heidelberg, Germany, **1996**.
[42] E. J. Baerends, O. V. Gritsenko, R. van Leeuwen, *Chemical Applications of Density Functional Theory*, American Chemical Society, Washington D. C., **1996**, vol. 629.
[43] E. J. Baerends, O. V. Gritsenko, *J. Phys. Chem. A* **1997**, *101*, 5383−5403.
[44] M. Grüning, O. V. Gritsenko, S. J. A. van Gisbergen, E. J. Baerends, *J. Chem. Phys.* **2001**, *114*, 652−660.
[45] P. R. T. Schipper, O. V. Gritsenko, S. J. A. van Gisbergen, E. J. Baerends, *J. Chem. Phys.* **2000**, *112*, 1344−1352.

[46] G. te Velde, F. M. Bickelhaupt, E. J. Baerends, C. Fonseca Guerra, S. J. A. van Gisbergen, J. G. Snijders, T. Ziegler, *J. Comput. Chem.* **2001**, *22*, 931−967.
[47] A. Becke, *Phys. Rev. A* **1988**, *38*, 3098−3100.
[48] J. P. Perdew, *Phys. Rev. B* **1986**, *33*, 8822; see also Erratum: *Phys. Rev. B 1986, 34*, 7406).
[49] S. J. A. van Gisbergen, J. G. Snijders, E.-J. Baerends, *Comput. Phys. Commun.* **1999**, *118*, 119−138.
[50] G. Gritzner, J. Kůta, *Pure Appl. Chem.* **1984**, *56*, 461−466.

Received October 3, 2003
Early View Article
Published Online March 9, 2004

